Methodology For Determination Of Space Control For 3D Reconstruction In Statscan Digital X-Ray Radiology Using Static Frame Model

Jacinta S. Kimuyu

Abstract: The methodology was designed to employ two positioning techniques in order to determine the three-dimensional control space of target points on static metal frame model to be used as space control data in 3D reconstructions in Statscan digital X-Ray imaging. These techniques were digital close-range photogrammetry and precise theodolite positioning method. The space coordinates for the target points were determined 3D using both techniques. Point positioning accuracy 0.5mm in root mean square error of X, Y and Z space coordinates was achieved. The outcome of the comparison of the results obtained from both methods were of satisfactory accuracy hence further use of the control space data in Stastcan imaging and 3D reconstruction.

1 Introduction

The experimental study investigations conducted were aimed at developing a methodology for determination of 3D space control for imaging on Statscan digital X-ray platform. There were two methods employed in the determination of the 3D space coordinates of target points designed on static metal frame model. The techniques used digital close-range photogrammetry method and precise theodolite positioning method. Point localization accuracy in 3D was established by comparing the results obtained from both methods. A photograph of the static metal frame taken with Nikon D100 camera is shown in Figure 1.

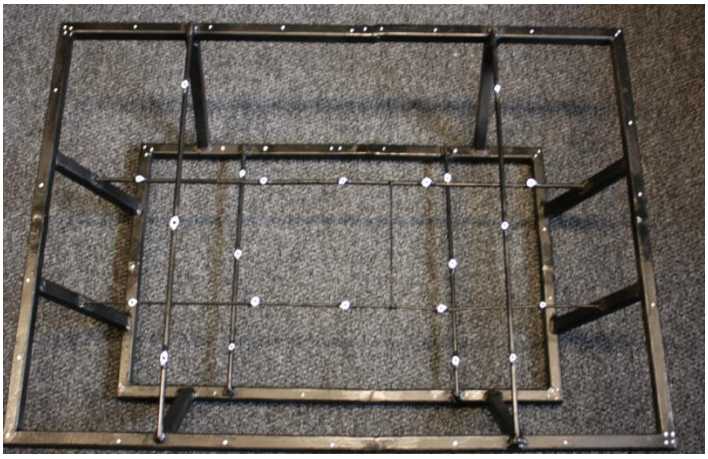

Figure 1 *Static metal frame model image*

Subsequently, the method used in determination of space control for the Statscan X-Ray modality should provide reliable data to be used in further 3D point localization in digital X-ray imaging. Control points for running the Direct Linear Transformation (DLT) reconstruction were chosen from the visible point targets on all scanned X-ray images of the static metal frame and used in the 3D reconstruction. Image coordinates of all the visible target points imaged on the static metal frame were measured and used together with the control coordinates to solve for the DLT parameters in Statscan X-Ray point localization. The solution obtained for the 11 DLT parameters were used to solve for the 3D coordinates of the new image points of interest.

2 Methodology

2.1 Space Control from Digital Close–Range Photogrammetry Method

Image acquisition was accomplished with Nikon D100 CCD Camera. The choice of camera for the project was favored by camera availability that led to its selection. The Nikon D100 is a "non-metric professional'' camera with Charge Coupled Detectors (CCD) and a sensor size of 3008 mm pixels in the horizontal direction and 2000 mm pixels in the vertical direction. Camera calibration is usually a pre-requisite procedure in photogrammetric projects, where amateur cameras have to be used. This rigorous task of determining the camera interior and exterior orientation parameters is inevitable. The technique used to calibrate the camera for the project was as reported by Marder (2005), whereby camera self-calibration involves the process of calculating the intrinsic parameters of the camera using only the information available in the images taken by the camera. For a number of images taken by the same camera with fixed internal parameters, correspondence between any three images is sufficient for the recovery of both the internal and external parameters. The cameras' interior orientation elements that need to be determined in the calibration process include the position for the principal point (x_0, y_0); the calibration focal length (calibration principal distance) which represents the distance of rear nodal point of the lens to the principal point of the photograph on the image plane (f) and finally the radial and decentering lens distortions (k_1, k_2, k_3) and (p_1, p_2) respectively (Brown, 1989). The exterior orientation parameters are also determined whereby such elements give the angular relationship $(\omega, \varphi, \kappa)$, between image space and the object space coordinate system, and the position of the camera front nodal point during exposure. The camera position in space is denoted by X_0, Y_0, Z_0. The camera self-calibrating bundle adjustment

technique is highly rigorous, with capability to achieve high accuracy in measurement, and is based on the least squares adjustment model. The stochastic model allows for errors in random observations, while the functional model consists of the collinearity equations. The collinearity equations are based on the assumption that the perspective center, the object and the corresponding image point all lie in a straight line. In most practical scenarios, this condition is not fulfilled due to inaccuracies in the lens/chip assembly and lens distortion. Each pair of observed image coordinates yields two collinearity equations along with the correction for lens distortion (Brown, 1989);

$$x_i - \delta_{x_i} = x_P - c\,\frac{m_{11}(X_i - X_C) + m_{12}(Y_i - Y_C) + m_{13}(Z_i - Z_C)}{m_{31}(X_i - X_C) + m_{32}(Y_i - Y_C) + m_{33}(Z_i - Z_C)} \quad \ldots(1)$$

$$y_i - \delta_{y_i} = y_P - c\,\frac{m_{21}(X_i - X_C) + m_{22}(Y_i - Y_C) + m_{23}(Z_i - Z_C)}{m_{31}(X_i - X_C) + m_{32}(Y_i - Y_C) + m_{33}(Z_i - Z_C)} \quad \ldots(2)$$

where,

(x, y) are the observed image coordinates;

δ_x and δ_y are the lens distortion;

(c) is the camera principal distance;

(x_P, y_P) are the image coordinates of the principal point;

(X_i, Y_i, Z_i) are the object space coordinates;

(X_C, Y_C, Z_C) are the perspective center coordinates in object space;

m_{ij} are the elements of an orthogonal matrix that defines the rotation between the image and the object coordinate system. The elements of the rotation matrix depend on the magnitude of the rotation angles about the axes, the type of the coordinate system (left or right handed), the rotation direction, and the rotation sequence.

2.1.1 Camera Calibration procedure for Nikon D100 by Australis software

The Australis software, (Fraser, 2001) was used for calibration of the Nikon D100 camera. The software employs self-calibrating bundle adjustment. The object to be measured was imaged from different horizontal and elevation positions and with varying orientations of the optical axes of the camera. The result was a convergent geometry with as many image coordinates for each target as the number of exposures on which the target is visible. The observations of discrete targeted points on the object are used as the data required for determination of the camera calibration parameters (Atkinson, 1996). For any successful self-calibration, the following criteria must be met according to Brown, 1989:

- At least three images should be taken using the camera to be calibrated, but several cameras can be calibrated at the same time.
- Both the interior geometry of the camera and the point to be measured on the object must remain stable during the measurement process.
- At least one image must have a roll angle that is significantly different from the others.
- A relatively large number of well distributed points should be used.

One of the digital images of the camera calibration test field used with reflective circular targets with contrasting black background on a wall is shown in Figure 2. The calibration test field is an established control field designed by the Geomatics Division at the University of Cape Town. For this project, 18 images of a test field with 73 reflective targets were used. To initiate the calibration process, the relative orientation method was used with two images taken from parallel camera axes.

Figure 2 *Calibration test field showing circular target points in black contrast (source: author's photograph)*

Figure 3 below shows the labeled target points of an image within Australis automatic point. The measured image coordinates for each point label have been displayed.

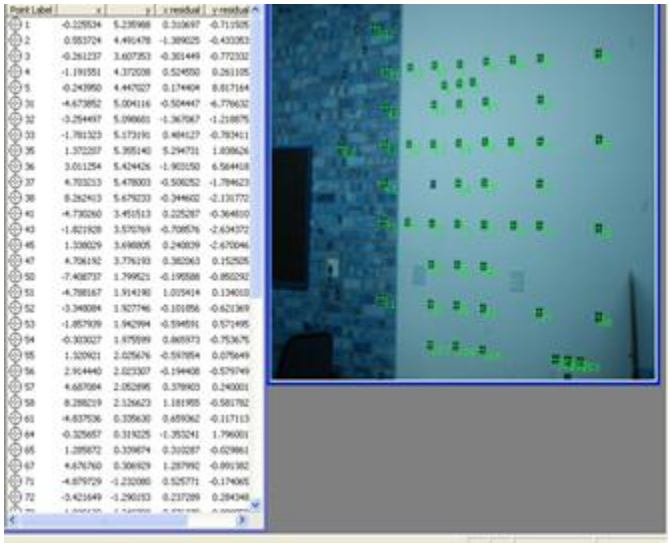

Figure 3 *Image view with labeled target points and the measured image coordinates.*

Figure 4 below is a display of the Nikon D100 28mm lens distortion profiles, as obtained from calibration using Australis software.

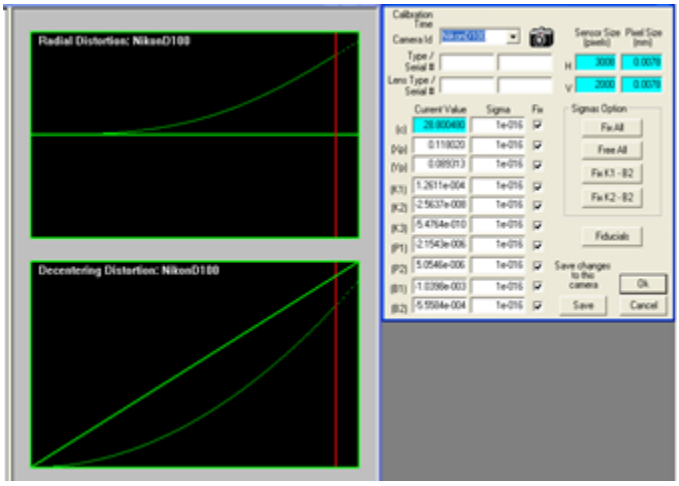

Figure 4 *Calibration Project view showing Camera calibration database, Radial lens distortion and Decentering distortion plots (the red vertical line limits the CCD format coverage).*

An important display tool in Australis is the 3D graphics view that displays the measured objects for visualization. This can be used after the points in the images forming the network have been measured. The graphics showing the point cloud generated after the bundle adjustment can then be displayed and the camera stations viewed (Figure 5).

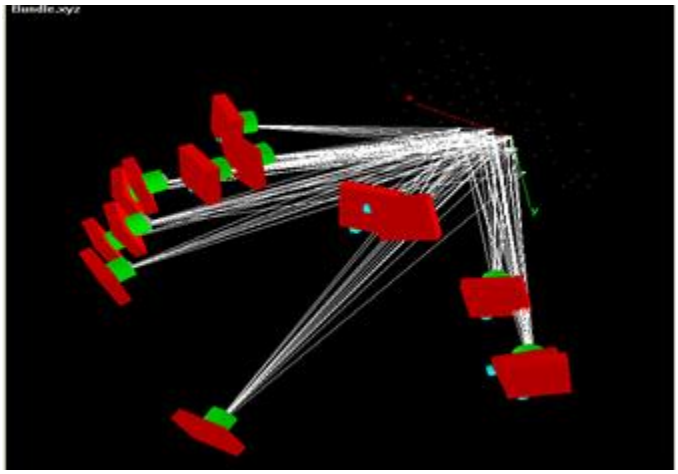

Figure 5 *Graphics Interface showing intersecting rays to selected points.*

2.1.2 Computing space coordinates of the static metal frame model

Further computation of the object space coordinates was done. The calibrated Nikon D100 28mm lens camera was used to photograph a 3D metal frame model. A local Cartesian coordinate system was used in this research. Scaling was done using the scalebar tool incorporated in Australis. The measured length and width of the metal frame formed the scalebar database. As reported by Fraser (2000), "an important feature of Australis is the ability to use scale data, either rigorously in the bundle adjustment as an observed distance of known a priori precision, as is needed to support self-calibration in multi-camera networks, or as a means to simply scale the final object space coordinates after the network adjustment". The 3D display of the reconstructed target points on the metal frame is shown in Figure 6.

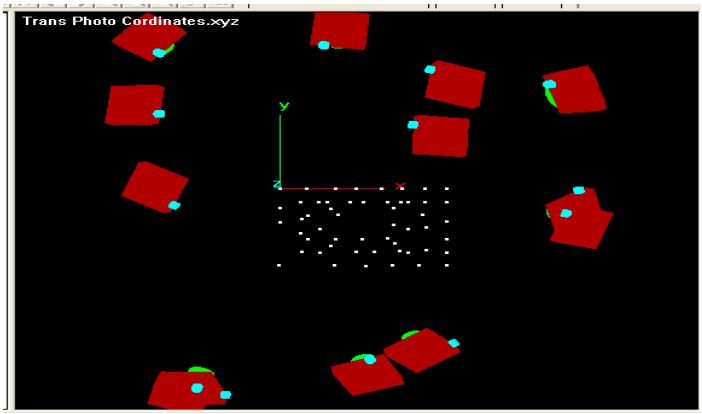

Figure 6 *Frame graphics showing reconstructed target points and the camera stations within Australis.*

The targets to be measured appear as white against black metal bar. The space coordinates of the targets on this frame were computed and later used as control and test points for reconstructing the 3D object coordinates from Lodox Statscan X-ray images. The black frame was designed with a series of 76 targets painted white for enhanced contrast in the images. A convergent network of 10 images incorporating orthogonal roll angle diversity was photographed at close-range. All targets on the images were measured, resection was performed and then a free-net bundle adjustment was executed. The results obtained from the bundle were the 3D space coordinates of the frame targets. The reconstructed space coordinates of the static metal frame have been tabulated with point positioning accuracy (Table 1).

Table 1 *Space coordinates of the big frame target points obtained from Australis bundle adjustment.*

Point label	X(mm)	Y(mm)	Z(mm)	Sigma X	Sigma Y	Sigma Z
1	296.9	-1147.9	-281.1	0.4	0.3	0.2
2	201	-1139.5	-278.4	0.3	0.2	0.2
3	101	-1128.4	-278.5	0.3	0.2	0.1
4	-32.4	-1116.1	-277.3	0.2	0.2	0.1
5	-178.3	-1103.8	-276.9	0.2	0.3	0.1
6	-282.7	-1094.8	-277.2	0.2	0.4	0.1
7	-288.1	-1158.9	-184.9	0.2	0.4	0.1
8	-292.9	-1227.2	-87.3	0.1	0.4	0.1
9	-298	-1293.5	5.7	0.1	0.4	0.1
10	-304	-1369	110.2	0.1	0.4	0.2
11	-308.8	-1432.2	200.8	0.1	0.3	0.2
12	-317.1	-1521.2	325.2	0.1	0.3	0.2
13	-327.7	-1603.6	439.8	0.2	0.3	0.3
14	-177.6	-1615.7	438.7	0.1	0.3	0.2
15	-69.8	-1626.5	438.9	0.1	0.4	0.2
17	256.3	-1661.9	441.4	0.1	0.6	0.1
19	272	-1491.2	202.9	0.2	0.5	0.1
20	282	-1398.2	70.7	0.2	0.4	0.1
21	287.5	-1315.5	-43.3	0.3	0.4	0.1

22	294.6	-1234.2	-158.4	0.3	0.3	0.2
31	193	-1246.9	-106.5	0.3	0.3	0.1
32	15.1	-1230.4	-106.6	0.2	0.2	0.1
33	-189	-1209.6	-104.7	0.2	0.3	0.1
34	-212.6	-1485	279.8	0.1	0.4	0.2
35	-7.8	-1503	276.9	0.1	0.4	0.2
36	166.2	-1520.1	275.7	0.2	0.5	0.1
51	111.4	-1423.3	-155.9	0.1	0.3	0.2
52	-30.6	-1412.8	-153.8	0.1	0.4	0.1
53	-159.7	-1399.6	-152.1	0.1	0.3	0.1
54	-171.9	-1601.4	128.9	0.2	0.5	0.1
56	111.5	-1629.9	127.9	0.1	0.4	0.1
62	-94.6	-1249	-225.1	0.1	0.3	0.1
65	-116.8	-1512.7	139.8	0.1	0.3	0.2
66	-124.3	-1606.7	275.4	0.1	0.4	0.2
67	59	-1622.2	279.3	0.1	0.4	0.1
68	68.9	-1541.4	150.9	0.2	0.5	0.3
69	73.5	-1455.1	36.9	0.1	0.3	0.1
70	75.6	-1376.8	-72.1	0.1	0.3	0.2
71	175	-1342	-301.2	0.1	0.3	0.2
72	-4.2	-1323.2	-299.8	0.1	0.2	0.2
73	-202.4	-1305.9	-299.3	0.1	0.3	0.1
74	-206.8	-1383.3	-188.6	0.1	0.3	0.1
75	-210.3	-1424.9	-128.4	0.1	0.3	0.1
76	-216.9	-1497.6	-23.9	0.2	0.3	0.1
77	-220.1	-1540.6	37.8	0.2	0.3	0.1
78	-224.5	-1612.7	136.6	0.2	0.3	0.1
79	-233.6	-1697.8	254.2	0.2	0.3	0.2
80	-102.5	-1709.4	252.1	0.2	0.4	0.1
81	5.9	-1720.9	252.3	0.2	0.4	0.1
82	153.9	-1734.3	249.3	0.1	0.5	0.1
85	167.1	-1557.5	6.9	0.1	0.4	0.1
86	170.6	-1502.9	-70.3	0.1	0.4	0.1
87	175.4	-1425.3	-182.5	0.1	0.3	0.2

2.2 Space Control from Precise Theodolite Observations Method

Precise theodolite positioning method was used to determine 3D coordinates of the same static metal frame model. The metal frame was positioned on a table for observation from three theodolite stations (A, B and C) as shown on Figure 7 below. The same number of target points were observed as identified in the digital photogrammetry technique. The theodolite stations formed an observation network of triangles to the target points. Forced centering was used with targets placed on two stations and the theodolite on the third station. At every station, horizontal and vertical angles were measured to the other two stations, then to every target point on the frame, and finally back to the stations to check instrument orientation. Prisms were used to electronically measure distances between the theodolite stations to get the baselines. The recorded data was used to compute the provisional point coordinates (x, y) from horizontal angles and distances. These provisional coordinates were adjusted by free network least squares adjustment programme (parametric case) to compute the final planimetric coordinates. The final adjusted x, y -coordinates were used in computing the distances required for the determination of the $z-$ coordinates. The observed vertical angles from the control stations to the points were used with the computed distances from the stations to the points. Table 2 gives the determined 3D positions of the frame target points.

Table 2 *Adjusted space coordinates of staticmetal frame target points determined by theodolite method.*

Point Label	X(mm)	Y(mm)	Z(mm)
1	3787.7	591.4	-718.3
2	3838.3	594.1	-637.3
3	3892.6	594.2	-551.6
4	3965	596.7	-439.4
5	4045.9	599.6	-318.4
6	4103.5	600.8	-231.1
7	4099.3	713.6	-230.1
8	4093.3	832.7	-229.9
9	4089.2	946.7	-229.7
10	4085.7	1075.4	-231
11	4080.2	1185.9	-229.9
12	4076.3	1338.9	-228.7
13	4074.4	1479.8	-225.2
14	3991.9	1476.6	-350.3
15	3932.2	1475.9	-441.3
17	3755.3	1477.6	-717.5
19	3764.3	1183.4	-718.4
20	3768.5	1022.1	-721.5
21	3773.2	881.7	-720.3
22	3778.6	740.7	-721.2
31	3821.1	796.2	-630.5
32	3919.7	798	-481.3
33	4029.2	800.3	-308.9
34	4013.5	1273.8	-307.7
35	3903.5	1268.6	-479.5
36	3808.7	1266.4	-626.1
51	4002.5	869.4	-672.1
52	4079.9	874.1	-554.2
53	4150.2	876.6	-444.4
54	4136.6	1220.4	-447.6
55	4060.8	1220.7	-563.6
56	3983.2	1218.1	-686.1
61	3963.7	724.8	-597.9
62	4056.3	722.5	-442.5
65	4044.7	1173.1	-442.5
66	4034.9	1337.3	-441
67	3933	1337.6	-592.6
68	3941.6	1186.5	-599.3
69	3947	1043.8	-596.5
70	3953	910.3	-592.9
72	4085.1	702	-576.2
73	4194.9	705.3	-410.3
74	4187.7	840.1	-410.6
75	4183.9	913.3	-410.1
77	4175.8	1115.5	-408.1
78	4171.8	1237.7	-409.3
79	4169.1	1382.8	-408.3
80	4097.3	1379.3	-518
81	4038.9	1379.2	-610.1
82	3959.3	1375	-734.8
85	3966.7	1075	-732.6
87	3978.9	844.3	-732.2

2.3 3D Coordinate Transformations

The object's local coordinate system was specified to be a right-handed system with the origin coinciding with theodolite station A, and the X-axis horizontal and along AC (see Figure 7; X-axis and AC are on the same vertical plane). In digital photogrammetry, the first camera station was the origin and the subsequent cameras were oriented relative to the first one. The first step was to convert the two systems into a coordinate system with the same axis orientation. This was accomplished by inverting the y -

coordinates of all the target points in the photogrammetric model. The resultant was a right-hand system that was used in all the subsequent 3D transformations.

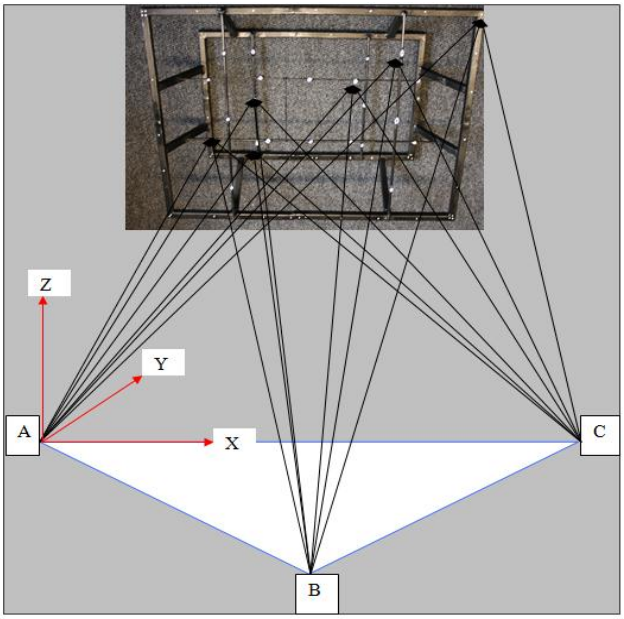

Figure 7 *Triangulation network from theodolite stations* A, B *and* C

Three-dimensional rigid body transformation of one system to the other preserves the shape of the model. The transformation helps in comparison by providing the discrepancies between the coordinate sets, represented by the residuals (v). Equation 3 below is used for three-dimensional similarity transformation.

$$\begin{bmatrix} X' \\ Y' \\ Z' \end{bmatrix} = sM \begin{bmatrix} X \\ Y \\ Z \end{bmatrix} + \begin{bmatrix} T_x \\ T_y \\ T_z \end{bmatrix} \quad \text{.....(3)}$$

Where;

s is the scale factor,

M is a 3-by-3 orthogonal rotation matrix,

$T_{x,}T_y$ and T_z are the translations along the three axes.

3 Results

The coordinates obtained from theodolite method were transformed into those obtained from digital photogrammetry using the 3D transformation tool of Australis software. The final transformation parameters used in the transformation are presented in Table 3.

Table 3 *Final rigid body transformation parameters.*

Transformation Parameter	Value	Std. Error
Xo (mm)	3125.7	0.37
Yo (mm)	144.2	0.34
Zo (mm)	199.9	0.39
Scale	1.00162	0.00021
Omega	-67.8	0.02
Phi	-30.8	0.01
Kappa	134.9	0.02

The Root Mean Square (RMS) of the XYZ residuals obtained from the transformed coordinates was 0.5 mm. The deduction from these results was that the digital photogrammetric procedure was satisfactorily accurate in determination of space control points that could be used in 3D localization for the Statscan digital X-ray system. The transformed coordinates and the coordinate differences in each point are tabulated in Table 4. Equation 4 was used in the determination of the RMS of the XYZ residuals.

$$RMS(XYZ) = \sqrt{\frac{\sum\left(DX^2 + DY^2 + DZ^2\right)}{3n}} \quad \text{.....(4)}$$

Where;

DX, DY and DZ are residuals in X, Y and Z respectively;

n is the total number of target points.

The theodolite observations were only done on the static metal frame to provide data to compare the accuracy obtained and to choose one method to be used in the X-Ray reconstruction. Eventually, the method chosen was the digital photogrammetry method which could be applied within the imaging room on the X-Ray platform to provide the required space control data.

Table 4 *Comparison between transformed theodolite coordinates (Xt,Yt,Zt) into Photo coordinates (Xp,Yp,Zp)*

Point label	Xp	Yp	Zp	Xt	Yt	Zt	DX	DY	DZ
1	296.9	-1147.9	-281.1	296.8	-1148.4	-281.6	0.1	0.5	0.5
2	201	-1139.5	-278.4	201.6	-1139	-279	-0.6	-0.5	0.6
3	101	-1128.4	-278.5	100.6	-1127.8	-278.9	0.4	-0.6	0.4
4	-32.4	-1116.1	-277.3	-32.6	-1115.4	-277.5	0.2	-0.7	0.2
5	-178.3	-1103.8	-276.9	-178	-1103.8	-277.4	-0.3	0	0.5
6	-282.7	-1094.8	-277.2	-282.3	-1094.5	-277.5	-0.4	-0.3	0.3
7	-288.1	-1158.9	-184.9	-288.1	-1159.5	-185.2	0	0.6	0.3
8	-292.9	-1227.2	-87.3	-292.6	-1227.6	-87.1	-0.3	0.4	-0.2
9	-298	-1293.5	5.7	-297.9	-1293.8	5.9	-0.1	0.3	-0.2
10	-304	-1369	110.2	-303.3	-1370	109.8	-0.7	1	0.4
11	-308.8	-1432.2	200.8	-308.2	-1432.7	201	-0.6	0.5	-0.2
12	-317.1	-1521.2	325.2	-317	-1522	325.3	-0.1	0.8	-0.1
13	-327.7	-1603.6	439.8	-328	-1604.1	439.6	0.3	0.5	0.2
14	-177.6	-1615.7	438.7	-178.4	-1616.6	438.7	0.8	0.9	0
15	-69.8	-1626.5	438.9	-69.9	-1626.8	439.1	0.1	0.3	-0.2
17	256.3	-1661.9	441.4	256.6	-1662.9	441.4	-0.3	1	0
19	272	-1491.2	202.9	271.5	-1491.3	202.1	0.5	0.1	0.8
20	282	-1398.2	70.7	282.2	-1398.2	70.4	-0.2	0	0.3
21	287.5	-1315.5	-43.3	287.8	-1315.7	-43.5	-0.3	0.2	0.2
22	294.6	-1234.2	-158.4	294.6	-1234.4	-158.9	0	0.2	0.5
31	193	-1246.9	-106.5	193.2	-1246.9	-107	-0.2	0	0.5
32	15.1	-1230.4	-106.6	14.7	-1230.9	-107.6	0.4	0.5	1
33	-189	-1209.6	-104.7	-188.7	-1209.9	-105.8	-0.3	0.3	1.1
34	-212.6	-1485	279.8	-211.8	-1485.3	279.9	-0.8	0.3	-0.1
35	-7.8	-1503	276.9	-8.3	-1504	276.3	0.5	1	0.6
36	166.2	-1520.1	275.7	165.8	-1520.7	275.4	0.4	0.6	0.3
51	111.4	-1423.3	-155.9	111.1	-1423.1	-155.2	0.3	-0.2	-0.7
52	-30.6	-1412.8	-153.8	-29.8	-1412.2	-152.7	-0.8	-0.6	-1.1
53	-159.7	-1399.6	-152.1	-159.8	-1399.7	-151.1	0.1	0.1	-1
54	-171.9	-1601.4	128.9	-172	-1600.5	128.8	0.1	-0.9	0.1
56	111.5	-1629.9	127.9	110.6	-1629	128	0.9	-0.9	-0.1
62	-94.6	-1249	-225.1	-94	-1248.5	-225.1	-0.6	-0.5	0
65	-116.8	-1512.7	139.8	-117	-1513.3	139.8	0.2	0.6	0
66	-124.3	-1606.7	275.4	-123.2	-1605.7	276.2	-1.1	-1	-0.8
67	59	-1622.2	279.3	59	-1622.1	279.3	0	-0.1	0
68	68.9	-1541.4	150.9	69.1	-1539.7	152.4	-0.2	-1.7	-1.5
69	73.5	-1455.1	36.9	73.1	-1455.4	36.8	0.4	0.3	0.1
70	75.6	-1376.8	-72.1	75.6	-1376.7	-71.4	0	-0.1	-0.7
72	-4.2	-1323.2	-299.8	-4	-1322.9	-299.7	-0.2	-0.3	-0.1
73	-202.4	-1305.9	-299.3	-202.6	-1306	-299.4	0.2	0.1	0.1
74	-206.8	-1383.3	-188.6	-207	-1383.1	-188.4	0.2	-0.2	-0.2
75	-210.3	-1424.9	-128.4	-210	-1424.7	-128	-0.3	-0.2	-0.4
77	-220.1	-1540.6	37.8	-220.1	-1540.7	37.9	0	0.1	-0.1
78	-224.5	-1612.7	136.6	-224.9	-1612.6	137	0.4	-0.1	-0.4
79	-233.6	-1697.8	254.2	-233.8	-1698	254.3	0.2	0.2	-0.1
80	-102.5	-1709.4	252.1	-102.8	-1708.9	252.6	0.3	-0.5	-0.5
81	5.9	-1720.9	252.3	5.7	-1720.8	252.5	0.2	-0.1	-0.2
82	153.9	-1734.3	249.3	153.4	-1734.3	249.4	0.5	0	-0.1
85	167.1	-1557.5	6.9	167.1	-1556.6	7.3	0	-0.9	-0.4
87	175.4	-1425.3	-182.5	174.8	-1424.7	-182.6	0.6	-0.6	0.1
								RMS(XYZ) = 0.5mm	

4 Discussion

The digital photogrammetry method was used to determine the space control coordinates for all the target points on static metal frame. Comparison of the data set obtained for space control with another set acquired using precise theodolite observations checked the accuracy obtained so as to choose one method to be used in Statscan X-Ray reconstruction. Since the comparison done using space coordinates from the metal frame resulted in satisfactory accuracy of 0.5mm RMS (XYZ), the digital photogrammetry procedure was adopted as reliable methodology for defining space control of objects to be scanned for 3D reconstruction in Statscan digital radiology system. The necessity was due to the limitation of the Statscan system to provide 3D images despite the commendable high speed scanning capability of the modality.

5 Conclusion

The methodology involved the use of digital photogrammetry positioning technique in order to provide the space positions for both the control and test points designed for 3D reconstruction in Statscan digital X-ray modality. The results obtained from 3D reconstruction using Australis software were compared to the space positions of the same target points obtained from precise theodolite positioning and found to be of reliable accuracy. Precise theodolite positioning method was used In order to provide an independent check for the space control data. The two data sets were compared by means of a three-dimensional similarity transformation of the digital photogrammetric coordinates into the positions derived by theodolite measurements. The rigid body transformation uses a mathematical model that preserves the relative space

positions of the points being transformed. Prior to the transformation of the coordinates from one system to the other, the object and target systems should both be in either right-hand or left-hand coordinate system. After computation and confirmation of agreement between the two methods with RMS (XYZ) of 0.5mm, one set of space control data, the digital photogrammetry set, was used in X-Ray 3D reconstruction.

Acknowledgement

The author expresses gratitude to the following organizations:-

- Deutscher Akademischer Austausch Diennst/DAAD e.V. German Academic Exchange Service, for research funding.
- Prof. Rüther, H. of Geomatics (UCT) for project supervision and provision of computing software.
- Greg Flash, Lodox (Pty) Ltd. research Manager, for assisting with data acquisition on the Statscan system and providing required research information.
- Prof. Kit Vaughan, Head of Biomedical Engineering Dept. (UCT); for allowing access to Statscan Digital Radiology System for Lodox (Pty) Ltd.

Author' Information

The author Dr. Jacinta S. Kimuyu is currently a Lecturer of Geospatial Engineering and Technology at The Technical University of Kenya. The study was accomplished in full fulfilment of MSc. degree in Engineering in Geomatics at the University of Cape Town (UCT) in South Africa in 2006. The full dissertation was published by UCT in terms of the non-exclusive license granted to UCT by the author. The copyright of the thesis vests in the author.

References and Bibliography

[1] Abdel-Aziz, Y.A., Karara, H.M., (1971); Direct linear transformation from comparator coordinates into object space coordinates in close-range photogrammetry, Proceedings of the ASP symposium on Close-Range Photogrammetry, pp 420-475.

[2] Adams, L.P., (1981); X-ray Stereo-photogrammetry locating the precise, three-dimensional position of image points. Medical and Biological Engineering and Computing, Vol. 19, pp 569 – 578.

[3] Atkinson, K.B., (1996); Close Range Photogrammetry and Machine Vision.

[4] Brown, D., (1989); A strategy for multi - camera On-the-job self calibration. Institut Fur Photogrammetrrie Stuttgart. www.vision.caltech.edu (accessed July, 2005).

[5] Douglas, T.S. et al., (2004); Three-dimensional point localization in low-dose X-ray images using Stereo-photogrammetry. Medical & Biological Engineering & Computing, Vol. 42, pp 37-43.

[6] Faig, W., (1976); Photogrammetric Potentials of Non-Metric cameras – Report of ISP Working Group V/2 18th ISP Congress, Helsinki. Photogrammetric Engineering and Remote Sensing, pp 47 – 49.

[7] El-Manadili, Y. and Novak, K., (1996); Precision rectification of SPOT imagery using the Direct Linear Transformation model, Photogrammetric Engineering and Remote Sensing, Vol. 62, pp 67-72.

[8] Faig, W. and Shih, T.Y., (1986); Critical Configuration of Object Space Control Points for the Direct Linear Transformation, Proceedings of the Symposium Real-Time Photogrammetry- A new challenge, ISPRS, Vol. 26, part 5, pp 23-29.

[9] Fraser, C.S. and Edmundson, K.L., (2000); Design and Implementation of a Computational Processing System for Off-Line Digital Close-Range Photogrammetry, ISPRS Journal of Photogrammetry & Remote Sensing, 55(2): pp94-104.

[10] Fraser, C.S., (2001); Australis User Manual, (University of Melbourne).

[11] Fritsch, D. and Stallmann, D., (200); Rigorous Photogrammetric Processing of high resolution Satellite Imagery, ISPRS, Vol. XXXIII, Armsterdam.

[12] Fryer, J.C., (1986); Lens Distortion for Close Range Photogrammetry, Proceedings of the Symposium Real-Time Photogrammetry- A new challenge, ISPRS, Vol. 26, part 5, pp30-37.

[13] Fryer, J.C., (1989); Camera Calibration in Non-Topographic Photogrammetry pp 59 – 69.

[14] Gonzales, R.C. and Woods, R.E., (2002); Digital Image Processing – International Edition (2nd Edition).

[15] Gonzales, R.C., Woods, R.E. and Eddins, S.L., (2004); Digital Image Processing using Matlab.

[16] Grossmann, W., (1975); Vermessungskunde II. Sammlung Göschen de Gruyter.

[17] Hicks, C.R., Turner, K.V. (Jr.), (1999); Fundamental Concepts in the Design of Experiments (5th Edition).

[18] Imaginis Corporation website, (1997-2006); History of Medical Diagnosis and Diagnostic Imaging,http://imaginis.com/faq/history.asp?mode=1 (updated: Feb 8, 2000), (retrieved March 13, 2006).

[19] ISPRS, (1986, June 16-19); Proceedings of the Symposium held in Ottawa, Canada. Real-Time Photogrammetry – A new challenge.

[20] Karara, H.M. (1989); Non-Topographic Photogrammetry (2nd Edition)

[21] Kasser, M. and Egels, Y., (2002); Digital Photogrammetry.

[22] South African Innovations, (2005, August 11); About South Africa, Science & Technology, Lifesaving SA innovation. http://www.southafrica.info/ess_info/sa_glance/scitech/statscan.htm (retrieved April 19, 2006).

[23] Lodox website; http://www.lodox.com/

[24] Marder, M., (2005, March); Comparison of Calibration Algorithms for a Low-Resolution, Wide Angle, 3D Camera. Master of Science Thesis, Stockholm, Sweden, IR – SB – EX – 0511.

[25] Marzan, G.T. and Karara, H.M., (1976, January); "Rational Design for Close Range Photogrammetry"; A report on a study sponsored by the National Science Foundation – as a part of research Grant GK-11655; Civil Engineering Studies-Photogrammetry Series No. 43; University of Illinois at Urbana-Chamaign (Urbana, Illinois 61801), pp 156-185.

[26] Mikhail, E.M., Bethel, J.S. and McGlone, J.C., (2001); Introduction to Modern Photogrammetry.

[27] Montgomery, D.C., (1976, 1984); Design and Analysis of Experiments (2nd Edition).

[28] Parsaye, K. and Chignell, M., (1993); Intelligent Database tools and Applications - Hyperinformation Access, Data Quality, Visualization and Automatic Discovery.

[29] Pennsylvania State University web site (1993); A Century of Radiology; A project of Radiology Centennial, Inc http://www.x-ray.hmc.psu.edu/rci/centennial.html/ (accessed March 18, 2006)

[30] Rüther, H., (2005, APG313S); Numerical Methods in Geomatics lecture notes (unpublished).

[31] Savopol, F. and Armenakis, C., (1998); Modelling of the IRS-IC Satellite Pan stereo imagery using DLT approach, International Archives of Photogrammetry and Remote Sensing, Vol. 32, part 4, pp511-514, Stuttgurt, Germany.

[32] Scheelke, M., Potgieter, H. and Mattieu de Villiers, (2005, February) (paper); "System characterization of the STATSCAN full body slit scanning radiography machine: Theory and experiment." Proceedings of SPIE Medical Imaging, San Diego.

[33] Tiggelen, R., JBR-BTR, (2002) 85: pp266-270; Historical Article, In search for the Third Dimension: From Radio stereoscopy to three-dimensional Imaging, http://www.radiology-museum.be/pdf/article_0081.pdf (accessed March 18, 2006)

[34] Van Geems, (1995) – A two-dimensional projective transformation approach to solve for 3D Coordinates from CT surviews, PhD. Dissertation, pp 44-47 and pp 192-194.

[35] Veress, et al., (1979); Analytical Approach to X-ray Photogrammetry. Photogrammetric Engineering and Remote Sensing, 43 (12):1503-1510.

[36] Veress, S.A. and Karara, H.M., (1989); X-ray Photogrammetry, System, and Applications (pp 167-186 of Non – Topographic Photogrammetry).

[37] Williams, H.P., (2003); Model Building in Mathematical Programming (4th Edition).

[38] Wolf, P.R. and Dewitt, B.A., (1974, 1983, 2000); Elements of Photogrammetry with Applications in GIS (3RD Edition).

[39] Wolf, P.R. and Ghilani, C.D., (1997); Adjustment Computations, Statistics and Least Squares in Surveying and GIS.